Intense fluorescence of Au_{20}

Chongqi Yu,[1] Wolfgang Harbich,[1] Luca Sementa,[2] Luca Ghiringhelli,[3] Edoardo Aprá,[4] Mauro Stener,[5] Alessandro Fortunelli,[2] and Harald Brune[1,a)]
[1]*Institute of Physics, Ecole Polytechnique Fédérale de Lausanne (EPFL), CH-1015 Lausanne, Switzerland*
[2]*CNR-ICCOM and IPCF, Consiglio Nazionale delle Ricerche, Via G. Moruzzi, 1-56124 Pisa, Italy*
[3]*Fritz-Haber-Institut der Max-Planck-Gesellschaft, Faradayweg 4-6, 14195 Berlin, Germany*
[4]*Environmental Molecular Sciences Laboratory, Pacific Northwest National Laboratory, Richland, Washington 99352, USA*
[5]*Dipartimento di Scienze Chimiche e Farmaceutiche, Università di Trieste, 34127 Trieste, Italy*

(Received 27 April 2017; accepted 10 July 2017; published online 15 August 2017)

Ligand-protected Au clusters are non-bleaching fluorescence markers in bio- and medical applications. Here we show that their fluorescence can be an intrinsic property of the Au cluster itself. We find a very intense and sharp fluorescence peak located at $\lambda = 739.2$ nm (1.68 eV) for Au_{20} clusters in a Ne matrix held at 6 K. The fluorescence reflects the Highest Occupied Molecular Orbital-Lowest Unoccupied Molecular Orbital (HOMO-LUMO) diabatic bandgap of the cluster. Au_{20} shows a very rich absorption fine structure reminiscent of well defined molecule-like quantum levels. These levels are resolved since Au_{20} has only one stable isomer (tetrahedral); therefore our sample is mono-disperse in cluster size and conformation. Density-functional theory (DFT) and time-dependent DFT calculations clarify the nature of optical absorption and predict both main absorption peaks and intrinsic fluorescence in fair agreement with experiment. *Published by AIP Publishing.* [http://dx.doi.org/10.1063/1.4996687]

I. INTRODUCTION

Gold clusters and gold nanoparticles have attracted considerable interest in fundamental research and technological applications. This started with their astonishing properties as heterogeneous catalysts[1–3] and went on with the discovery of their electronic[4] and more recently their optical properties.[5,6] In particular, the fluorescence of Au clusters and nanoparticles has shown great potential in a variety of disciplines, such as switchable fluorescence in Au-nanoparticle/DNA/rotaxane hybrid nanostructures,[7] enhanced fluorescence from dye molecules by Au nanoparticles,[8] non-bleaching fluorescence of gold nanoparticles for the application in cancer cell imaging,[9] multiphoton fluorescence in human insulin Au nanodots,[10] molecular fluorescence of Au/SiO_2 core-shell nanoparticles,[11] and label-free fluorescence on protein-protected Au clusters.[12] A fundamental understanding of the origin of fluorescence in Au nanoclusters is of critical importance for applications in bioimaging and photonics.

Since all previous studies were either performed on ligand-protected or protein-encapsulated Au clusters,[12–16] it has remained unclear whether the fluorescence is intrinsic to the Au cluster or emerging from its interaction with ligands, and the considerable theoretical effort dedicated to the simulation of absorption spectra[17–21] and fluorescence[22] has not answered this question. For bare Au clusters, experiments were limited to cluster sizes below the relevant one. Absorption spectra exist only up to a size of 9 atoms[23–26] and fluorescence measurements only up to a size of 3 atoms.[22,25]

Here we report fluorescence and absorption measurements of Au_{20}. For this size, the tetrahedral structure is by far the most favorable one[27] such that only this single conformer exists at our measurement temperature of 6 K. We use Ne matrices that exhibit weak van der Waals interactions with the clusters leading to a known offset in energies, but leaving the cluster properties unchanged with respect to the gas phase. We find that Au_{20} exhibits intense and sharp fluorescence at a wavelength of 739.2 nm (1.68 eV). This fluorescence can best be excited at 536.8 nm (2.31 eV) and 394.9 nm (3.14 eV); however also excitation in the entire UV-to-visible range leads to fluorescence. We present first-principles calculations that trace the origin of fluorescence back to molecule-like single particle excitations that are appreciably intermixed by Coulomb and spin-orbit effects. Our results prove that fluorescence is an intrinsic property of Au_{20} suggesting that in many of the above mentioned studies, the fluorescence can go back to the Au core itself rather than to the ligands.

II. EXPERIMENTAL

We used a custom designed experimental setup to produce samples of neutral Au_{20} clusters dilutely dispersed into solid Ne matrices. For this, we coupled a sputter gas aggregation cluster source[28] to a newly designed cluster ion beam line consisting of a conical octupole[29] focussing the clusters, followed by a radiofrequency coupled quadrupole guiding them, and finally by a high mass extranuclear quadrupole for mass selection. This setup selects cluster ions up to 16 000 amu with an electronically controllable mass resolution. We created a flux of Au_{20} cations with a kinetic energy of 20 eV and directed it onto a super polished aluminum mirror held at 6 K while dosing Ne that condenses onto the mirror and

a)harald.brune@epfl.ch

forms the matrix. The cluster ions are efficiently neutralized by an electron cloud formed in front of the matrix. The excess energy from the neutralization process is coupled to the matrix avoiding fragmentation. The cluster flux and Ne partial pressure were adjusted to yield a cluster to rare gas atom ratio of typically $1/10^4$ optimizing signal to noise in the optical measurement while ensuring that mutual interactions between the clusters remain negligible. We grew a Au_{20}/Ne matrix with a thickness of 50 μm in 2 h. The width of the matrix was 2 mm.

Optical absorption was measured in transmission through the 2 mm wide matrix using a deuterium or tungsten lamp as source and collecting the transmitted light with a 400 μm core optical fiber and then analyzing it in a spectrometer with a liquid-nitrogen-cooled charge coupled device as detector in a range of 250 nm–1.0 μm (for a more detailed description, see Ref. 30). The Au_{20} absorption was obtained by subtracting a Ne matrix reference spectrum from the one of the Au_{20}/Ne matrix. For fluorescence spectra, we excited with diode lasers (λ = 266, 375, 473, 532 nm) normal to the surface of the Ne matrix and collected the fluorescence light perpendicular to the excitation (through the matrix) by focusing on a fiber to which the same spectrometer and detector as in the absorption spectra are attached. Excitation spectra were recorded by monochromatic detection perpendicular to the matrix at the fluorescence wavelength while varying the wavelength of the source using one of the lamps mentioned above and monochromatizing their light.

III. RESULTS AND DISCUSSION

A. Experiments for Au_{20}/Ne

Figure 1 shows optical absorption, excitation, and fluorescence spectra measured on mass-selected, neutral, and mono-conformal Au_{20} clusters dilutely embedded in solid Ne at 6 K. The clusters show a very rich absorption spectrum with many large and small characteristic absorption peaks that were labeled for comparison with the energies in Table I. These peaks are superimposed onto a continuously increasing background as the energy increases. This background is consistent with the optical absorption of bulk gold[31] and inherent to basically all experimental optical spectra of ligand stabilized Au clusters at room temperature, which, apart from the Au surface plasmon, show broad structures superimposed onto that background.[20,32] In our experiment, the spectroscopic signatures are distinct and narrow. The most prominent absorption peak occurs at 3.14 eV (395 nm, k), and the peaks of medium intensity are located at 2.31 eV (536.8 nm, b), 3.20 eV (387.5 nm, l), 3.99 eV (310.8 nm, p), 4.11 eV (301.7 nm, q), 4.52 eV (274.3 nm, t), and 5.0 eV (248 nm, u). The weak interaction with the matrix, the monodispersity, the monoconformality, and the low temperature clearly reveals the information on the quantum states of the cluster[20] (see Sec. III B).

Excitation of Au_{20} at all energies above 1.8 eV results in a very intense and sharp fluorescence peak at 739.2 nm (1.68 eV) with a bandwidth (FWHM) of about 35 nm (0.08 eV). Note that a group of much weaker fluorescence peaks is present. These peaks are conform to the absorption

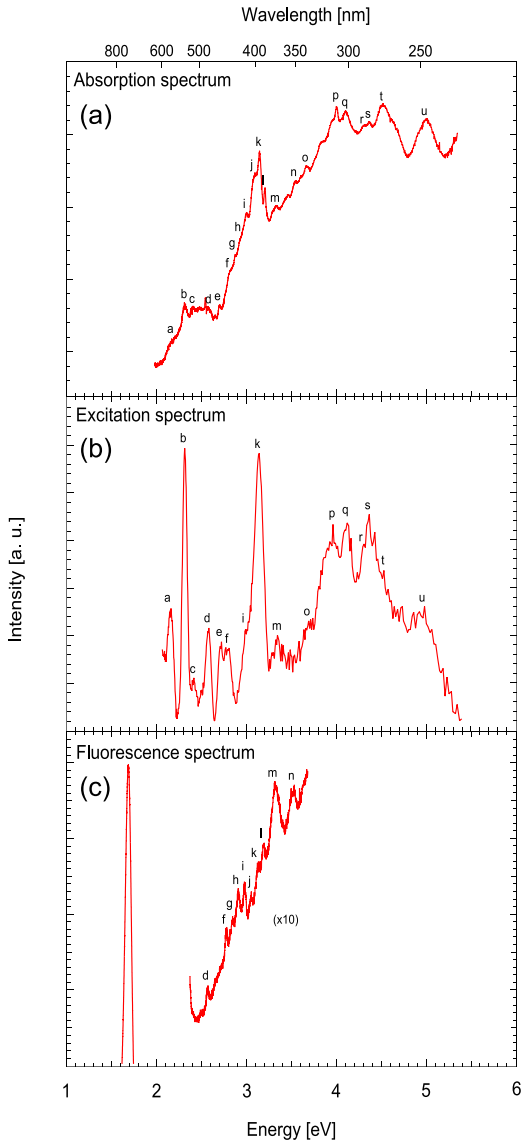

FIG. 1. (a) Au_{20}/Ne absorption spectrum (broad band illumination, spectral detection). (b) Excitation spectrum (monochromatic excitation, monochromatic detection at the main fluorescence line of 739.2 nm). (c) Fluorescence spectrum (excitation at 266 nm, spectral detection).

spectrum and show up only upon excitation with sufficiently high photon energy, for 266 nm, see Fig. 1(c), and 375 nm (not shown). Based on the observation of a strong fluorescence at 739.2 nm (1.68 eV), excitation spectra have been recorded [Fig. 1(b)]. The main transitions associated with this fluorescence channel are at 536.8 nm (2.31 eV, b) and 395 nm (3.14 eV, k), while weaker transitions are at 574.1 nm (2.16 eV, a), 310.8 nm (3.99 eV, p), 301.7 nm (4.11 eV, q), and 284.4 nm (4.36 eV, s). Compared to the absorption spectrum, the excitation spectrum provides exactly the same positions and approximately the same line widths on all transitions, however, without the continuous background absorption up to 4 eV. The excitation spectrum only mirrors the fluorescing states at 739.2 nm (1.68 eV) and therefore reflects a subset of electronic transitions of the absorption spectrum in Fig. 1(a). The missing transitions are attributed to emission dark states, i.e., to non fluorescing states in the Au cluster. It is worth mentioning that very few emission dark channels are found:

TABLE I. Transitions in the optical absorption of Au_{20}. Bold numbers highlight strong transitions.

Peaks	Energy (eV)	Wavelength (nm)
a	2.16	574.1
b	**2.31**	**536.8**
c	2.41	514.5
d	2.58	480.5
e	2.71	457.5
f	2.78	446.0
g	2.85	435
h	2.91	426
i	2.98	416
j	3.06	405
k	**3.14**	**394.9**
l	**3.2**	**387.5**
m	3.34	371.3
n	3.54	350.3
o	3.69	336.0
p	**3.99**	**310.8**
q	**4.11**	**301.7**
r	4.31	287.7
s	4.36	284.4
t	**4.52**	**274.3**
u	**5.0**	**248.0**

this is consistent with the configurational mixing deduced from TDDFT.

Assuming that the fluorescence involves the lowest excited state in the cluster, i.e., there are no lower-energy emission dark channels (see discussion below), we have a precise measurement of the diabatic bandgap of Au_{20} which is 1.68 eV. This value is consistent with optical bandgaps obtained from ligand stabilized Au clusters counting only the metal core,[32] i.e., Au_{n-m} where n is the nominal cluster size and m is the number of sulfur bonded Au atoms. It is noteworthy that the optical bandgap for the tetrahedral Au_{20} in Ne with the full valence electron count fits almost perfectly to the value proposed by Jin[32] for icosahedral Au particles.

Fluorescence has so far been observed for free or quasi free Au clusters only up to the size of $n = 3$.[25,33] For Au_2, the fluorescence peak was at 809 nm (1.83 eV) and had a width of $\Delta E = 0.2$ eV;[33] for Au_3, there were three fluorescence peaks located at 529 nm (2.34 eV), 579 nm (2.14 eV), and 809 nm (1.53 eV).[25] Compared to the fluorescence reported for these small clusters, Au_{20} has a fluorescence peak with significantly higher intensity. Ligand stabilized Au clusters can show strong fluorescence depending on the size and the nature of the ligands.[32] For example, Wu *et al.* showed fluorescence in $Au_{25}(SCH_2CH_2Ph)^-_{18}$ at 750 nm with 150 nm linewidth.[15] Xu *et al.* found fluorescence for polydisperse Au nanoclusters on BSA (bovine serum albumin) from 650 to 700 nm with 100 nm linewidth.[14] Wen *et al.* reported fluorescence of Au_{25}/BSA at 690 nm with 120 nm linewidth,[34] and finally, Liu *et al.* presented fluorescence on human insulin Au nanodots at about 700 nm with 150 nm linewidth.[10] The important and yet open question is whether the fluorescence in these ligand-protected Au nanoclusters is intrinsic to the metal core or to the cluster ligand system. Our spectra on pure Au_{20} clusters show a much smaller linewidth in absorption and fluorescence. This is at least partially attributed to the low temperature of the cluster under study (T = 6 K compared to 300 K). It is to mention that low temperature (77 K) absorption measurements on ligand stabilised Au_{144} show much narrower absorption peaks compared to the room temperature spectrum of the identical system.[20] The resemblance of our data with the ligand stabilized clusters strongly suggests that the fluorescence found in the biologically relevant systems can be Au mediated.

B. DFT and TDDFT modeling and comparison with experiment

A first-principles-based theoretical investigation of fluorescence of Ne-embedded gold clusters represents a difficult computational task due to the interplay of several physical effects: mixing of molecule-like and preplasmonic excitations, spin-orbit coupling, influence of Ne matrix, role of van der Waals (vdW) dispersion interactions, and crossing of potential energy surfaces of different excited states. To face this challenge, we adopt a combination of different methods and codes.

We focus first on the long-standing problem of quantifying the effect of the Ne matrix on the structure and optical properties of embedded Au clusters. For this, we considered (i) tetrahedral (T_d) Au_{20} and (ii) a $Au_{20}Ne_{100}$ cluster with the 100 Ne atoms arranged according to a homomorphic tetrahedral layer surrounding Au_{20}. We relaxed the structure using density-functional theory (DFT) employing a generalized-gradient-approximation Perdew-Burke-Ernzerhof (PBE) exchange-correlation (xc-)functional.[35] VdW interactions were introduced by adding to the DFT energy a sum over $C_6[n]/R^6$ tails, with C_6 coefficients derived in two different ways: either via the Tkatchenko-Scheffler (vdW-TS) scheme, i.e., from the self-consistent electron density and reference values for the free atoms,[36] or via the more recent range-separated many-body dispersion (MBD) approach.[37] The accuracy of the vdW-TS approach for predicting the structural properties of Au clusters interacting with rare-gas atoms has been validated against higher-level first-principles methods and experiment,[38] and represents the current state-of-the-art modeling of such systems. The MBD approach is more recent and has been shown to be in general superior to the vdW-TS approach, in particular, for heterogenous systems. This can be understood because MBD includes many-body contributions and the self-consistent screening of the atomic polarizability. The FHI-aims package[39] was used in these calculations, and the optimized geometries at the PBE-MBD level are reported in the supplementary material (the PBE-vdW-TS geometries and associated TDDFT spectra turn out to be very similar so they are not explicitly reported). As a major conclusion of this analysis, the effect of the Ne matrix on the geometry of Au_{20} in the electronic ground state turns out to be negligible, with differences in coordinate values less than 0.01 Å.

The optical absorption spectra of Au_{20} and $Au_{20}Ne_{100}$ were then simulated at the optimised DFT/PBE-MBD geometries via time-dependent DFT (TDDFT) calculations in the Casida formalism[40] using the hybrid B3LYP xc-functional[41] at the scalar-relativistic (SR) level, and the results are reported

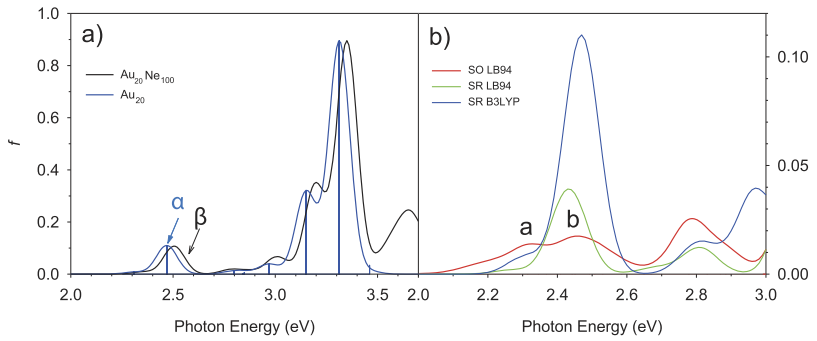

FIG. 2. TDDFT-simulated absorption spectrum of Au_{20} and $Au_{20}Ne_{100}$ at the DFT/PBE-MBD geometries: (a) Au_{20} (both discrete and smoothed, blue line) and $Au_{20}Ne_{100}$ (smoothed, black lines) using the B3LYP xc-functional at the scalar-relativistic (SR) level; (b) Au_{20} using B3LYP at the scalar-relativistic (SR) level (smoothed, blue line), LB94 xc-functional at the SR level (smoothed, green line), and LB94 xc-functional including spin-orbit (SO) coupling (both discrete and smoothed, red lines). In (a), the α and β SR peaks on which fluorescence has been explicitly simulated are indicated, while in (b), the peaks indicated as a and b correspond to the assignment of the corresponding experimental absorption features. Smoothed profiles are obtained by convolution with Gaussian functions of FWHM = 0.12 eV. Note that the photon energy range is different in (a) and (b) panels to better highlight the broadening due to SO coupling in the region below 3 eV.

in Fig. 2(a). Previous theoretical work showed that the position and intensity of predicted absorption peaks of Au_{20} are rather sensitive to the theoretical approach employed, especially the xc-functional.[42] Local density or gradient-corrected xc-functionals severely underestimate the intensity of absorption peaks below 3 eV, and a proper description of the Coulombic tail of the potential is crucial to assure a reasonable description of the optical response of Au clusters.[42] Neglecting the moment spin-orbit (SO) effects, TDDFT/B3LYP predicts absorption peaks below 3 eV at 2.22 eV, 2.42 eV, and 2.88 eV, and three major peaks between 3.08 and 3.39 eV towering the spectrum (see Table S1 of the supplementary material for more information and an analysis of the excited states in terms of single-particle components). Figure 2(a) demonstrates that the effect of the Ne matrix on the absorption of Au_{20} is minor, basically amounting to a small blue-shift of the peak positions (a charge compression effect on the excited orbitals). Note that for computational reasons, the number of calculated roots of the Casida matrix, thus the range of excitation energies, is limited. The TDDFT/B3LYP calculations in Fig. 2(a) are performed using a double-zeta-plus-polarization basis set and the NWChem package[43] at the SR level.

To better understand the nature of the low-lying excited electronic states, we report in Fig. 3 the single-particle orbitals of Au_{20} in its electronic SR ground state as a function of energy and occupation, labeled according to the irreducible representations of the T_d symmetry group (more details are provided in Table S1 and Fig. S1 of the supplementary material where the orientation of Au_{20} used to plot orbital densities is shown). We then highlight in particular the two lowest excited states at 2.22 eV and 2.42 eV, respectively, that are explicitly indicated as α and β both in Fig. 3 and in Fig. 2(a), and mainly correspond to $16e \rightarrow 30t2$ and $29t2 \rightarrow 30t2$ single-particle transitions (see Table S1).

Spin-orbit (SO) effects are known to be potentially important in the optical response of Au clusters.[44] Being unable to include SO coupling in the B3LYP calculations for technical reasons, we estimate its influence by using the semi-local Coulomb-tail-corrected SAOP xc-functional[45] and the ADF package.[46] Although SAOP is less accurate than B3LYP or other hybrid xc-functionals, SAOP predicts for Au_{20} an optical absorption profile qualitatively consistent with these xc-functionals. The SAOP absorption spectra up to 3 eV with and without SO coupling are reported in Fig. 2(b). As expected, the SR peaks split into several peaks after the introduction of SO coupling, thus producing an overall spectral appearance in good agreement with the rich experimental absorption shown in Fig. 1(a), whose continuous background is so interpreted as due to SO splitting of SR absorption intensity into a multitude of peaks.

Moreover, by comparison with Fig. 1(a) and Table I, we can single out SO features in Fig. 2(b) that can be associated with the (a) and (b) experimental peaks. These SO features derive basically from a mixing of the SR peaks at 2.22 eV

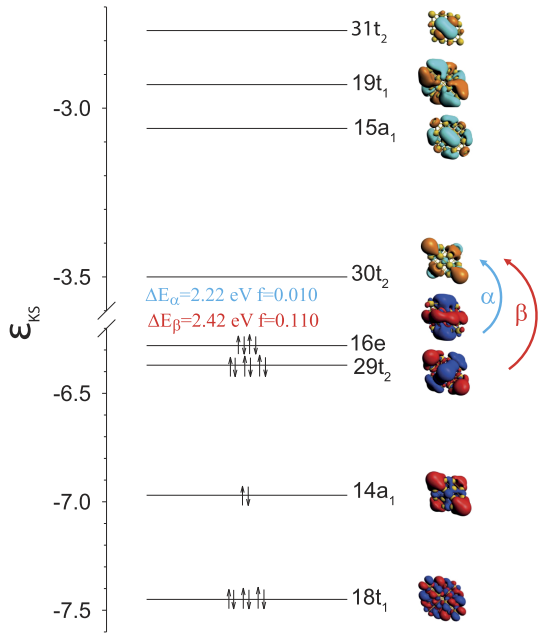

FIG. 3. Au_{20} DFT/B3LYP single-particle molecular orbitals as a function of energy and occupation, labeled according to the irreducible representations of the T_d symmetry group. The main single-particle components of the two lowest-energy TDDFT/B3LYP excited states at the scalar-relativistic (SR) level with their excitation energy and oscillator strength are also indicated with blue and red arrows for the α and β excitation, respectively.

and 2.42 eV, respectively, while the experimental major peaks (j,k,l) can analogously be put into correspondence with features deriving from the three major SR peaks between 3.08 and 3.39 eV.

In summary, the comparison between observed and simulated absorption spectra demonstrates that (i) the Ne matrix does not qualitatively influence the structure and electron dynamics in Au_{20}, and (ii) the generally fair agreement between TDDFT predictions (including the previous literature[42]) and experiment makes us confident in using a TDDFT approach also for investigating fluorescence phenomena. For technical reasons, we are only able to do this at the TDDFT/B3LYP scalar-relativistic (SR) level on the two low-energy α and β absorption peaks.

We thus investigate the evolution/relaxation of the first two α and β excited states of bare Au_{20}, i.e., the very weak transition at 2.22 eV and the more intense absorption at 2.42 eV (named α and β). We recall that these SR states originate SO states that can be put into correspondence with (a,b)-peaks at 2.31 eV in the experimental excitation spectrum of Fig. 1(b). The geometry of these two excited states has been relaxed at the TDFFT/B3LYP level using the NWChem code. At the T_d equilibrium ground state geometry, both α and β are threefold-degenerate electronic states belonging to the t_1 irreducible representation of the T_d symmetry group. An analysis of the eigenvector of the Hessian matrix more strongly coupled to energy minimization shows that α relaxes its energy by lowering the symmetry from T_d to D_2, smoothly ending up in a local energy minimum in which the excitation energy from the electronic ground state is 1.99 eV (the Cartesian coordinates of the relaxed geometry are reported in the supplementary material). β initially relaxes its energy by lowering the symmetry from T_d to C_2. However, after an initial decrease in energy by $\approx$0.1 eV, the minimization process gets trapped in regions of the potential energy surface exhibiting a complicated crossing of excited states and conical intersections (the Cartesian coordinates of one of these crossing geometries are reported in the supplementary material). Notably, in these regions, excited states originating from components of the α and β triply degenerate multiplets appreciably mix, with mixing coefficients (i.e., expansion coefficients of β-like excited states onto single-particle excitations originally pertaining to α-like excited states and vice versa) ranging from 0.1 to 0.3. It is therefore reasonable to assume that surface hopping from β-like to α-like excited states easily occurs in these regions, followed by a smooth relaxation to the D_2 local minimum of the lowest-energy E_1-like component, which finally fluoresces in the electronic ground state. It can be noted that the weaker oscillator strength of α-like states delays spontaneous fluorescent emission. We thus finally predict a shift between β absorption at 2.42 eV and α fluorescence of 0.43 eV, in fair agreement with experimental observations.

IV. CONCLUSION

We present the first optical absorption, excitation, and fluorescence spectra of the tetrahedral Au_{20}. In our experiments, Au_{20} is embedded in a solid neon matrix at 6 K. Our first-principles calculations reveal that this matrix has no effect on the cluster structure, its only effect is a slight blue shift of the absorption spectrum. The absorption spectrum exhibits a series of sharp discrete transitions on a smooth background that increases with energy and whose overall appearance is similar to the background found for ligand-protected Au clusters at low temperatures. Au_{20} exhibits intense and sharp fluorescence. Our results strongly suggest that the metal core in ligand-protected clusters plays a central role in the fluorescence. The fluorescence in Au_{20} is shown to involve mostly Highest Occupied Molecular Orbital-Lowest Unoccupied Molecular Orbital (HOMO-LUMO) and HOMO(−1)-LUMO excitations, which are well separated in the tetrahedral ground-state geometry, but strongly interact and mix when excited-state relaxation deforms it. It is finally notable that fluorescence emission—as shown by TDDFT response calculations—involves the lowest excited state (i.e., there are no energetically lower dark emission channels). Therefore the fluorescence peak provides a precise measure of the diabatic bandgap which is 1.68 eV for Au_{20}.

SUPPLEMENTARY MATERIAL

See supplementary material for additional information on the optical absorption excitations of Au_{20} in terms of single-particle components and associated induced-density plots, and the geometry of Au_{20} and $Au_{20}Ne_{100}$ systems in their electronic ground and two lowest excited states.

ACKNOWLEDGMENTS

Experimental work has been supported by the Swiss National Science Foundation. Computational research was performed in part using EMSL, a DOE Office of Science User Facility sponsored by the Office of Biological and Environmental Research and located at Pacific Northwest National Laboratory, and PNNL Institutional Computing at Pacific Northwest National Laboratory. Support from the CINECA supercomputing centre within the ISCRA program is also gratefully acknowledged.

[1] M. Haruta, N. Yamada, T. Kobayashi, and S. Iijima, J. Catal. **115**, 301 (1989).
[2] M. Valden, X. Lai, and D. W. Goodman, Science **281**, 1647 (1998).
[3] M. Haruta, Nature **437**, 1098 (2005).
[4] C. Zhang, Y. He, H. P. Cheng, Y. Q. Xue, M. A. Ratner, X. G. Zhang, and P. Krstic, Phys. Rev. B **73**, 125445 (2006).
[5] T. G. Schaaff and R. L. Whetten, J. Phys. Chem. B **104**, 2630 (2000).
[6] P. Zhang, X. Yang, Y. Wang, N. Zhao, Z. Xiong, and C. Huang, Nanoscale **6**, 2261 (2014).
[7] A. Cecconello, C.-H. Lu, J. Elbaz, and I. Willner, Nano Lett. **13**, 6275 (2013).
[8] J. H. Guo, L. Z. Liu, X. B. Zhu, X. L. Wu, and P. K. Chu, Appl. Phys. Lett. **104**, 141910 (2014).
[9] H. He, C. Xie, and J. Ren, Anal. Chem. **80**, 5951 (2008).
[10] C.-L. Liu, T.-M. Liu, T.-Y. Hsieh, H.-W. Liu, Y.-S. Chen, C.-K. Tsai, H.-C. Chen, J.-W. Lin, R.-B. Hsu, T.-D. Wang, C.-C. Chen, C.-K. Sun, and P.-T. Chou, Small **9**, 2103 (2013).
[11] P. Reineck, D. Gomez, S. H. Ng, M. Karg, T. Bell, P. Mulvaney, and U. Bach, ACS Nano **7**, 6636 (2013).
[12] Y. Wang, Y. Wang, F. Zhou, P. Kim, and Y. Xia, Small **8**, 3769 (2012).
[13] S. Wang, X. Meng, A. Das, T. Li, Y. Song, T. Cao, X. Zhu, M. Zhu, and R. Jin, Angew. Chem., Int. Ed. **53**, 2376 (2014).

[14]Y. Xu, J. Sherwood, Y. Qin, D. Crowley, M. Bonizzoni, and Y. Bao, Nanoscale **6**, 1515 (2014).
[15]Z. Wu and R. Jin, Nano Lett. **10**, 2568 (2010).
[16]X. Wen, P. Yu, Y.-R. Toh, X. Ma, S. Huang, and J. Tang, Nanoscale **5**, 10251 (2013).
[17]C. M. Aikens, J. Phys. Chem. A **113**, 10811 (2009).
[18]S. Malola, L. Lehtovaara, J. Enkovaara, and H. Häkkinen, ACS Nano **7**, 10263 (2013).
[19]J. C. Idrobo, W. Walkosz, S. Yip, S. Oeguet, J. Wang, and J. Jellinek, Phys. Rev. B **76**, 205422 (2007).
[20]H. C. Weissker, H. B. Escobar, V. D. Thanthirige, K. Kwak, D. Lee, G. Ramakrishna, R. L. Whetten, and X. López-Lozano, Nat. Commun. **5**, 3785 (2014).
[21]G. Barcaro, L. Sementa, A. Fortunelli, and M. Stener, Phys. Chem. Chem. Phys. **17**, 27952 (2015).
[22]K. L. Dimuthu, M. Weerawardene, and C. M. Aikens, J. Am. Chem. Soc. **138**, 11202 (2016).
[23]G. A. Bishea and M. D. Morse, J. Chem. Phys. **95**, 5646 (1991).
[24]W. Harbich, S. Fedrigo, J. Buttet, and D. Lindsay, Z. Phys. D **19**, 157 (1991).
[25]S. Fedrigo, W. Harbich, and J. Buttet, J. Chem. Phys. **99**, 5712 (1993).
[26]S. Lecoultre, A. Rydlo, C. Felix, J. Buttet, S. Gilb, and W. Harbich, J. Chem. Phys. **134**, 074302 (2011).
[27]J. Li, X. Li, H. J. Zhai, and L. S. Wang, Science **299**, 864 (2003).
[28]I. M. Goldby, B. von Issendorff, L. Kuipers, and R. E. Palmer, Rev. Sci. Instrum. **68**, 3327 (1997).
[29]M. A. Rottgen, K. Judai, J. M. Antonietti, U. Heiz, S. Rauschenbach, and K. Kern, Rev. Sci. Instrum. **77**, 013302 (2006).
[30]F. Conus, J. T. Lau, V. Rodrigues, and C. Félix, Rev. Sci. Instrum. **77**, 113103 (2006).
[31]P. B. Johnson and R. W. Christy, Phys. Rev. B **6**, 4370 (1972).
[32]R. Jin, Nanoscale **7**, 1549 (2015).
[33]S. Lecoultre, A. Rydlo, C. Félix, and W. Harbich, Eur. Phys. J. D **52**, 187 (2009).
[34]X. Wen, P. Yu, Y. Toh, A. Hsu, Y. Lee, and J. Tang, J. Phys. Chem. C **116**, 19032 (2012).
[35]J. P. Perdew, K. Burke, and M. Ernzerhof, Phys. Rev. Lett. **77**, 3865 (1996).
[36]A. Tkatchenko and M. Scheffler, Phys. Rev. Lett. **102**, 073005 (2009).
[37]A. Ambrosetti, A. M. Reilly, R. A. DiStasio, and A. Tkatchenko, J. Chem. Phys. **140**, 18A508 (2014).
[38]L. M. Ghiringhelli, P. Gruene, J. T. Lyon, D. M. Rayner, G. Meijer, A. Fielicke, and M. Scheffler, New J. Phys. **15**, 083003 (2013).
[39]V. Blum, R. Gehrke, F. Hanke, P. Havu, V. Havu, X. Ren, K. Reuter, and M. Scheffler, Comput. Phys. Commun. **180**, 2175 (2009).
[40]M. Casida, *Recent Advances in Density-Functional Methods* (World Scientific, 1995), p. 155.
[41]A. D. Becke, J. Chem. Phys. **98**, 5648 (1993).
[42]B. Anak, M. Bencharif, and F. Rabilloud, RSC Adv. **4**, 13001 (2014).
[43]R. A. Kendall, E. Aprà, D. E. Bernholdt, E. J. Bylaska, M. Dupuis, G. I. Fann, R. J. Harrison, J. Ju, J. A. Nichols, J. Nieplocha, T. P. Straatsmab, T. L. Windus, and A. T. Wong, Comput. Phys. Commun. **128**, 260 (2000).
[44]D. Jiang, M. Kühn, Q. Tang, and F. Weigend, J. Phys. Chem. Lett. **5**, 3286 (2014).
[45]O. Gritsenko, P. Schipper, and E. Baerends, Chem. Phys. Lett. **302**, 199 (1999).
[46]C. F. Guerra, J. G. Snijders, G. te Velde, and E. J. Baerends, Theor. Chem. Acc. **99**, 391 (1998).

Supplementary Information for "Intense fluorescence of Au_{20}"

Chongqi Yu[1], Wolfgang Harbich[1], Luca Sementa[2], Luca Ghiringhelli[3], Edoardo Aprà[4], Mauro Stener[5], Alessandro Fortunelli[2], Harald Brune[1,*]

[1] *Institute of Physics, Ecole Polytechnique Fédèrale de Lausanne (EPFL), CH-1015 Lausanne, Switzerland*

[2] *CNR-ICCOM, Consiglio Nazionale delle Ricerche, via G. Moruzzi, 1 - 56124 - Pisa - Italy*

[3] *Fritz-Haber-Institut der Max-Planck-Gesellschaft, Faradayweg 4-6 - 14195 - Berlin – Germany*

[4] *Environmental Molecular Sciences Laboratory, Pacific Northwest National Laboratory - Richland - WA 99352 – USA*

[5] *Dip. di Scienze Chimiche e Farmaceutiche, Università di Trieste - 34127 - Trieste - Italy*

To complement the analysis in the main text, here we provide additional information on :

1. the optical absorption excitations of Au_{20} in terms of single-particle components and associated induced-density plots
2. the geometry of Au_{20} and $Au_{20}Ne_{100}$ systems in their electronic ground states as predicted via a DFT/PBE-MBD approach and the geometry of Au_{20} in its electronic ground state and two lowest excited states as predicted via a DFT/B3LYP approach

For technical reasons of use of symmetry, the DFT/B3LYP analysis in Table S1 and Figure S1 is performed using the ADF package [1], but the TDDFT results coincide with those obtained using the NWChem package [2] which is used throughout this work in the relaxation of excited states. The induced electron density or equivalently the transition density in Figure S1 is defined in equation 5.4.5 of ref. [3].

References

[1] C. Fonseca Guerra, J. G. Snijders, G. te Velde, E. J. Baerends, "Towards an order-N DFT method" *Theor. Chem. Acc.* **99**, 391-403 (1998)

[2] R. A. Kendall, E. Aprà, D. E. Bernholdt, E. J. Bylaska, M. Dupuis, G. I. Fann, R. J. Harrison, J. Ju, J. A. Nichols, J. Nieplocha, T. P. Straatsma, T. L. Windus, A. T. Wong, "High performance computational chemistry: An overview of NWChem a distributed parallel application" *Comput. Phys. Commun.* **128**, 260-283 (2000)

[3] R. McWeeny, *Methods of Molecular Quantum Mechanics*, 2nd edn, Academic Press, London, 1989

Table S1. Analysis of the main excitations in the TDDFT/B3LYP scalar-relativistic spectrum of Au_{20} in terms of single-particle components. See Figure 3 of the main text for the definition of single-particle orbitals.

Transition	E (eV)	*f*	Composition
1	2.22	0.0096	97% $16e \rightarrow 30t_2$
2	2.42	0.118	85% $29t_2 \rightarrow 30t_2$
3	2.70	0.0203	90% $29t_2 \rightarrow 15a_1$
4	2.82	0.00005	77% $16e \rightarrow 19t_1$ + 14% $29t_2 \rightarrow 19t_1$
5	2.88	0.0136	41% $16e \rightarrow 19t_1$ + 46% $29t_2 \rightarrow 19t_1$
6	2.99	0.00089	50% $14a_1 \rightarrow 30t_2$ + 22% $16e \rightarrow 31t_2$
7	3.08	0.0504	77% $29t_2 \rightarrow 31t_2$
8	3.25	0.718	49% $18t_1 \rightarrow 30t_2$ + 12% $14a_1 \rightarrow 30t_2$
9	3.39	0.668	44% $18t_1 \rightarrow 30t_2$ + 9% $14a_1 \rightarrow 30t_2$

Figure S1. Induced electron density relative to electronic excited states of Au_{20} predicted at the TDDFT/B3LYP scalar-relativistic level as reported in Table S1.

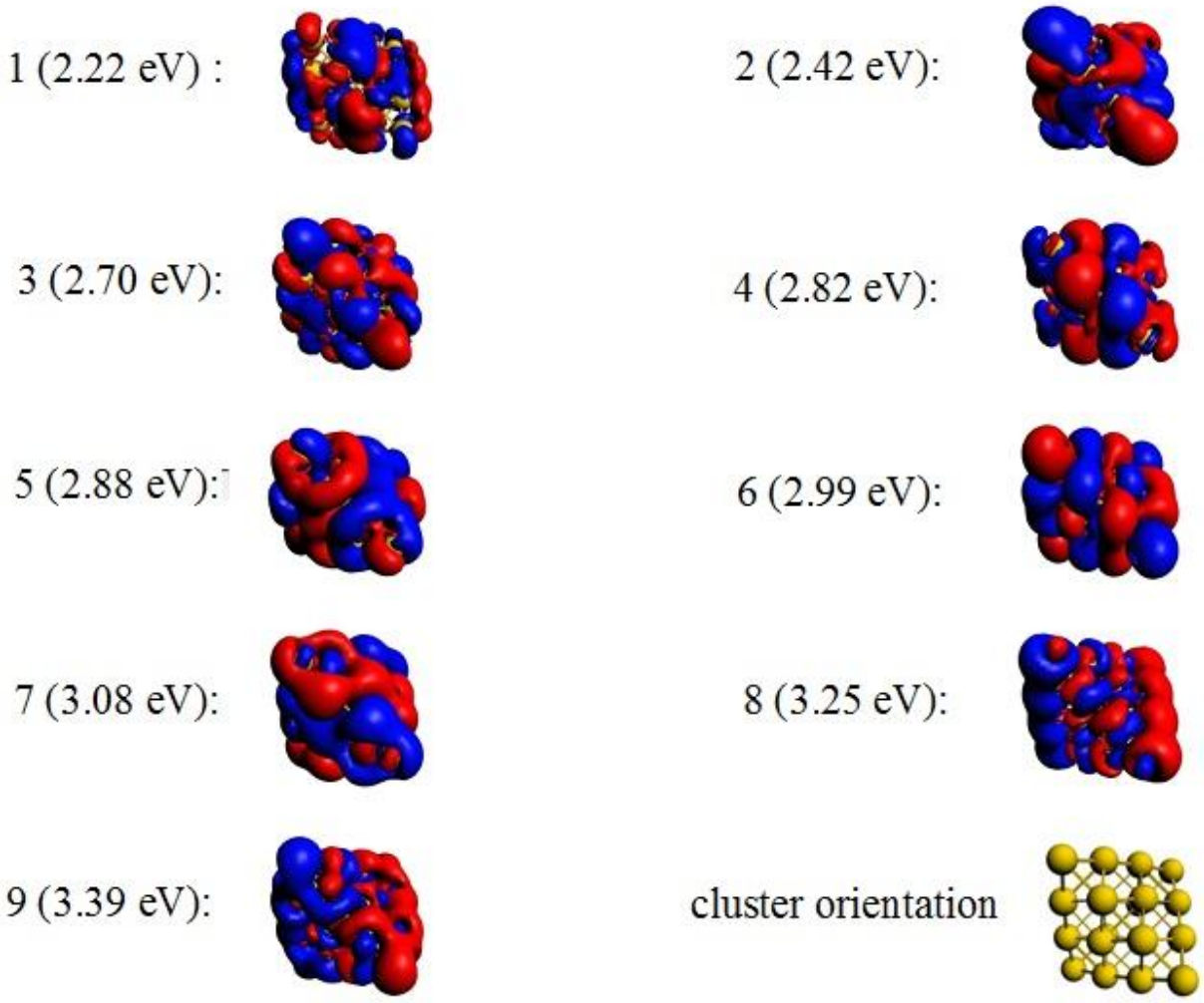

Cartesian coordinates of Au_{20} in its electronic ground state relaxed at the DFT/PBE-MBD level

Au	2.86187	2.86187	-2.86187
Au	3.03114	0.94689	-0.94689
Au	3.03114	-0.94689	0.94689
Au	2.86187	-2.86187	2.86187
Au	0.94689	3.03114	-0.94689
Au	1.10909	1.10909	1.10909
Au	0.94689	-0.94689	3.03114
Au	-0.94689	3.03114	0.94689
Au	-0.94689	0.94689	3.03114
Au	-2.86187	2.86187	2.86187
Au	0.94689	0.94689	-3.03114
Au	1.10909	-1.10909	-1.10909
Au	0.94689	-3.03114	0.94689
Au	-1.10909	1.10909	-1.10909
Au	-1.10909	-1.10909	1.10909
Au	-3.03114	0.94689	0.94689
Au	-0.94689	-0.94689	-3.03114
Au	-0.94689	-3.03114	-0.94689
Au	-3.03114	-0.94689	-0.94689
Au	-2.86187	-2.86187	-2.86187

Cartesian coordinates of $Au_{20}Ne_{100}$ in its electronic ground state relaxed at the DFT/PBE-MBD level

Au	2.85392	-2.85392	2.85392
Au	-1.09068	1.09068	-1.09068
Au	2.85392	2.85392	-2.85392
Au	3.02465	0.94368	-0.94368
Au	3.02465	-0.94368	0.94368
Au	0.94368	3.02465	-0.94368
Au	1.09068	1.09068	1.09068
Au	0.94368	-0.94368	3.02465
Au	-0.94368	3.02465	0.94368
Au	-0.94368	0.94368	3.02465
Au	-2.85392	2.85392	2.85392
Au	0.94368	0.94368	-3.02465
Au	1.09068	-1.09068	-1.09068
Au	0.94368	-3.02465	0.94368
Au	-1.09068	-1.09068	1.09068
Au	-3.02465	0.94368	0.94368
Au	-0.94368	-0.94368	-3.02465
Au	-0.94368	-3.02465	-0.94368
Au	-3.02465	-0.94368	-0.94368
Au	-2.85392	-2.85392	-2.85392
Ne	7.38477	-1.07509	1.07509
Ne	5.92422	1.58311	1.58311
Ne	3.81606	3.81606	1.62314
Ne	1.58311	5.92422	1.58311
Ne	-1.07509	7.38477	1.07509
Ne	5.89325	-3.70575	0.68959
Ne	-3.70575	5.89325	0.68959
Ne	3.70575	-5.89325	0.68959
Ne	-5.89325	3.70575	0.68959
Ne	1.07509	-7.38477	1.07509
Ne	-1.58311	-5.92422	1.58311
Ne	-3.81606	-3.81606	1.62314
Ne	-5.92422	-1.58311	1.58311
Ne	-7.38477	1.07509	1.07509
Ne	7.38477	1.07509	-1.07509
Ne	5.89325	3.70575	-0.68959
Ne	3.70575	5.89325	-0.68959
Ne	1.07509	7.38477	-1.07509
Ne	5.92422	-1.58311	-1.58311
Ne	-1.58311	5.92422	-1.58311
Ne	3.81606	-3.81606	-1.62314
Ne	-3.81606	3.81606	-1.62314
Ne	1.58311	-5.92422	-1.58311
Ne	-5.92422	1.58311	-1.58311
Ne	-1.07509	-7.38477	-1.07509
Ne	-3.70575	-5.89325	-0.68959
Ne	-5.89325	-3.70575	-0.68959
Ne	-7.38477	-1.07509	-1.07509
Ne	7.64859	3.23754	-3.23754
Ne	5.45465	5.45465	-3.22126
Ne	3.23754	7.64859	-3.23754
Ne	5.89325	0.68959	-3.70575

Ne	0.68959	5.89325	-3.70575
Ne	3.81606	-1.62314	-3.81606
Ne	-1.62314	3.81606	-3.81606
Ne	1.62314	-3.81606	-3.81606
Ne	-3.81606	1.62314	-3.81606
Ne	-0.68959	-5.89325	-3.70575
Ne	-5.89325	-0.68959	-3.70575
Ne	-3.23754	-7.64859	-3.23754
Ne	-5.45465	-5.45465	-3.22126
Ne	-7.64859	-3.23754	-3.23754
Ne	7.67564	5.43827	-5.43827
Ne	5.43827	7.67564	-5.43827
Ne	5.45465	3.22126	-5.45465
Ne	3.22126	5.45465	-5.45465
Ne	3.70575	0.68959	-5.89325
Ne	0.68959	3.70575	-5.89325
Ne	1.58311	-1.58311	-5.92422
Ne	-1.58311	1.58311	-5.92422
Ne	-0.68959	-3.70575	-5.89325
Ne	-3.70575	-0.68959	-5.89325
Ne	-3.22126	-5.45465	-5.45465
Ne	-5.45465	-3.22126	-5.45465
Ne	-5.43827	-7.67564	-5.43827
Ne	-7.67564	-5.43827	-5.43827
Ne	7.64139	7.64139	-7.64139
Ne	5.43827	5.43827	-7.67564
Ne	3.23754	3.23754	-7.64859
Ne	1.07509	1.07509	-7.38477
Ne	-1.07509	-1.07509	-7.38477
Ne	-3.23754	-3.23754	-7.64859
Ne	-5.43827	-5.43827	-7.67564
Ne	-7.64139	-7.64139	-7.64139
Ne	7.64859	-3.23754	3.23754
Ne	5.89325	-0.68959	3.70575
Ne	3.81606	1.62314	3.81606
Ne	1.62314	3.81606	3.81606
Ne	-0.68959	5.89325	3.70575
Ne	-3.23754	7.64859	3.23754
Ne	5.45465	-5.45465	3.22126
Ne	-5.45465	5.45465	3.22126
Ne	3.23754	-7.64859	3.23754
Ne	0.68959	-5.89325	3.70575
Ne	-1.62314	-3.81606	3.81606
Ne	-3.81606	-1.62314	3.81606
Ne	-5.89325	0.68959	3.70575
Ne	-7.64859	3.23754	3.23754
Ne	7.67564	-5.43827	5.43827
Ne	5.45465	-3.22126	5.45465
Ne	3.70575	-0.68959	5.89325
Ne	1.58311	1.58311	5.92422
Ne	-0.68959	3.70575	5.89325
Ne	-3.22126	5.45465	5.45465
Ne	-5.43827	7.67564	5.43827
Ne	5.43827	-7.67564	5.43827
Ne	3.22126	-5.45465	5.45465
Ne	0.68959	-3.70575	5.89325
Ne	-1.58311	-1.58311	5.92422

Ne	-3.70575	0.68959	5.89325
Ne	-5.45465	3.22126	5.45465
Ne	-7.67564	5.43827	5.43827
Ne	7.64139	-7.64139	7.64139
Ne	5.43827	-5.43827	7.67564
Ne	3.23754	-3.23754	7.64859
Ne	1.07509	-1.07509	7.38477
Ne	-1.07509	1.07509	7.38477
Ne	-3.23754	3.23754	7.64859
Ne	-5.43827	5.43827	7.67564
Ne	-7.64139	7.64139	7.64139

Cartesian coordinates of Au_{20} in its electronic ground state relaxed at the DFT/B3LYP level

Au	2.93630007	2.93630007	2.93630007
Au	-1.13346203	-1.13346203	-1.13346203
Au	-2.93630007	-2.93630007	2.93630007
Au	-0.96466216	-0.96466216	3.14298745
Au	0.96466216	0.96466216	3.14298745
Au	-0.96466216	-3.14298745	0.96466216
Au	1.13346203	-1.13346203	1.13346203
Au	3.14298745	0.96466216	0.96466216
Au	0.96466216	-3.14298745	-0.96466216
Au	3.14298745	-0.96466216	-0.96466216
Au	2.93630007	-2.93630007	-2.93630007
Au	-3.14298745	-0.96466216	0.96466216
Au	-1.13346203	1.13346203	1.13346203
Au	0.96466216	3.14298745	0.96466216
Au	1.13346203	1.13346203	-1.13346203
Au	0.96466216	-0.96466216	-3.14298745
Au	-3.14298745	0.96466216	-0.96466216
Au	-0.96466216	3.14298745	-0.96466216
Au	-0.96466216	0.96466216	-3.14298745
Au	-2.93630007	2.93630007	-2.93630007

Cartesian coordinates of Au_{20} in its electronic first excited state E_1 relaxed at the DFT/B3LYP level

Au	2.93793713	3.03822207	2.93969461
Au	-1.20446374	-1.13139170	-1.20394166
Au	-2.93793713	-3.03822207	2.93969461
Au	-1.00603628	-0.95638911	3.13142783
Au	1.00603628	0.95638911	3.13142783
Au	-0.98036924	-3.03645629	0.97959279
Au	1.20446374	-1.13139170	1.20394166
Au	3.13238437	0.95726888	1.00729580
Au	0.98036924	-3.03645629	-0.97959279
Au	3.13238437	-0.95726888	-1.00729580
Au	2.93793713	-3.03822207	-2.93969461
Au	-3.13238437	-0.95726888	1.00729580
Au	-1.20446374	1.13139170	1.20394166
Au	0.98036924	3.03645629	0.97959279
Au	1.20446374	1.13139170	-1.20394166
Au	1.00603628	-0.95638911	-3.13142783
Au	-3.13238437	0.95726888	-1.00729580
Au	-0.98036924	3.03645629	-0.97959279
Au	-1.00603628	0.95638911	-3.13142783
Au	-2.93793713	3.03822207	-2.93969461

Cartesian coordinates of Au_{20} in its electronic second excited state E_2 relaxed at the DFT/B3LYP level up to the crossing point among several potential energy surfaces

Au	2.98861663	2.99055380	2.88716046
Au	-1.12172575	-1.12983711	-1.15306552
Au	-2.98861663	-2.99055380	2.88716046
Au	-0.98313766	-0.96962666	3.09833242
Au	0.98313766	0.96962666	3.09833242
Au	-0.95401734	-3.09367529	0.97175912
Au	1.24113861	-1.24518394	1.26339802
Au	3.08944170	0.95127916	0.97306641
Au	1.00892659	-3.10229763	-0.96507756
Au	3.09640134	-1.00208763	-0.97766803
Au	2.96970570	-2.97794645	-2.97437337
Au	-3.08944170	-0.95127916	0.97306641
Au	-1.24113861	1.24518394	1.26339802
Au	0.95401734	3.09367529	0.97175912
Au	1.12172575	1.12983711	-1.15306552
Au	0.98151904	-0.97565993	-3.12353193
Au	-3.09640134	1.00208763	-0.97766803
Au	-1.00892659	3.10229763	-0.96507756
Au	-0.98151904	0.97565993	-3.12353193
Au	-2.96970570	2.97794645	-2.97437337